Journal of Solid State Electrochemistry (2021) 25:2115–2125
https://doi.org/10.1007/s10008-021-04958-2

ORIGINAL PAPER

Hollow BiOBr/reduced graphene oxide hybrids encapsulating hemoglobin for a mediator-free biosensor

Hafiz Akif Munir[1] · Hui Liu[1] · Jiaojiao Gao[1] · Lingyan Pang[1] · Kai Guo[1] · Congyue Duan[1]

Received: 31 December 2020 / Revised: 15 April 2021 / Accepted: 22 April 2021 / Published online: 13 May 2021

Abstract

For the construction of a mediator-free biosensor, hollow BiOBr microspheres (H-BiOBr MS) were hydrothermally synthesized and combined with reduced graphene oxide (H-BiOBr/rGO hybrids); then, the hybrids were applied to immobilize hemoglobin (Hb) on the surface of a glassy carbon electrode. The structure and morphology of the H-BiOBr MS and H-BiOBr/rGO hybrids were examined using scanning electron microscopy (SEM), X-ray diffraction (XRD) and transmission electronic microscopy (TEM). The experimental results demonstrate that the hollow H-BiOBr/rGO hybrid material has a larger specific surface area and better biocompatibility, which is beneficial for immobilization of hemoglobin (Hb) and furthermore allows proteins to become more stable and bioactive. In addition, the as-prepared modified electrode hybrids can improve effectively the direct electron transfer of Hb. As a result, the hollow BiOBr/rGO microspheres-based H_2O_2 biosensors exhibit a wide linear range of 0.1 to 420 μM and extremely low limit of detection 0.02 μM. The drafted biosensor holds 93.7% of the preliminary feedback to H_2O_2 after 60-day storage. It is concluded that the mediator-free biosensors containing hollow BiOBr/rGO microspheres have wide applications in biomedicine and environmental analysis.

Keywords Biosensor · Hollow microsphere · Direct electron transfer · Hydrogen peroxide · Hemoglobin

Introduction

Over the last years, investigations demonstrate that a nanomaterial modified electrode possesses a particular impact on electrochemical determination and electrocatalysis [1–4]. Specifically, it may perform an essential and extraordinary role in a direct electrochemical biosensor [5–7]. An additional reconnaissance of direct electron transfer (DET) of redox proteins or enzymes may not just assist to realize the thermodynamic and intrinsic kinetic properties of proteins but also to determine the basis for fabricating mediator-free biosensors [8, 9]. Nevertheless, as a result of the denaturalization of proteins at the bare electrode surface as well as the profound burying of an electroactive center in the protein structure, this is complicated for proteins to realize the DET process on the bare electrode [10, 11]. Thus, it is renowned that the best morphology and structure of nanomaterials possess a substantial impact on the property of the immobilized enzyme that ascertains their effect in biosensors [12]. From a recent research, it has been indicated that to fabricate mediator-free biosensors and to immobilize enzymes, a succession of nanomaterials with special surface effect and good biocompatibility could be utilized [13]. Among them, hollow structural nanomaterials have drawn substantial attention in different applications of sensor because of its corresponding properties and unique structure, such as high specific surface area, well-defined interior voids, structural stability and high stability [14–17].

The bismuth oxyhalides BiOX (X=Cl, Br, I) has pulled significant attention in the area of environment protection and photocatalysis potential applications because of high chemical stability and extraordinary structure, as well as low cost and environmental friendliness [18–21]. Among many of these bismuth oxyhalides, BiOBr, which have a special layered structure and an effect of narrow band gap for visible-

✉ Hui Liu
liuhui@sust.edu.cn

✉ Lingyan Pang
panglingyan@sust.edu.cn

[1] School of Materials Science and Engineering, Shaanxi Key Laboratory of Green Preparation and Functionalization for Inorganic Materials, Shaanxi University of Science and Technology, Xi'an 710021, People's Republic of China

light response, possess an extensive application in the area of photocatalysis [22, 23]. The intrinsic layered structure endows high carrier mobility and small recombination possibility of photo generated charge carriers, which is beneficial to the electrochemical catalysis activity. Meanwhile, BiOBr nanostructures with various morphologies, possessing a good structural stability and biocompatibility, have been widely developed [24, 25]. Thus, a promising potential application for three-dimensional (3D) structured BiOBr nanophase materials is favored in the field of sensors.

However, same as the most inorganic nanomaterials used in immobilization of enzymes, there is an obvious disadvantage in its conductivity because of the interference of internal electronic fields. In order to enhance the conductivity properties of the electronic materials, graphene is usually used to make an extremely excellent support to improve the deficiency [26, 27]. Graphene, a two-dimensional material of sp^2 hybridization carbon atoms, is the thinnest as well as the strongest known material. It consists of a single layer of carbon atoms and is both pliable and transparent. In recent years, it has gained much attention owing to its extraordinary mechanical, electronic, magnetic, thermal and optical properties as well as large specific surface area [28–32]. Here, a unique hollow BiOBr microspheres (H-BiOBr MS) was designed and synthesized by a simple hydrothermal process and then combined with reduced graphene oxide (H-BiOBr/rGO hybrids) for fabricating a mediator-free biosensor. As an assistance for enzyme immobilization, this kind of three-dimensional H-BiOBr/rGO hybrids showed numerous benefits. Firstly, as shown in Scheme 1, this flower-like hollow structure of microsphere was sell-assembled by various thin nanosheets, and the intervals of nanosheets may become tunnels for enzymes to migrate to the inside of the microsphere. Simultaneously, few enzymes could be engrossed at the rGO exterior surrounding the microsphere. Secondly, to keep their enzymatic activity as well as stability, the interspaces among BiOBr nanosheets can offer a defensive microenvironment for the enzymes. Thirdly, the substrate may remain entangled by graphene with a high surface area due to the nanoscaled BiOBr nanosheets, which owns a huge surface area accessible for enzyme entanglement and provides accesses to the interspaces between BiOBr nanosheets. Lastly, absorption of substrate as well as enzyme in the constrained area would enhance an opportunity of efficient collisions among them [33]. Graphene with the extraordinary mobility of charge carriers may also become an extraordinary media of effective electrical communication between the electrode and the enzyme. Thus, such kind of H-BiOBr/rGO hybrids must be an encouraging assistance for enzyme immobilization and possess potential applications in biosensors.

In this paper, for construction of the H_2O_2 biosensor, hemoglobin (Hb) was chosen as a model redox protein. For the purpose of highlighting the benefits of the H-BiOBr/rGO hybrids as an assistance, the efficiency of a sensor consisting of Hb immobilized in the H-BiOBr/rGO hybrids microspheres was compared with that of sensors on the basis of pure BiOBr microspheres.

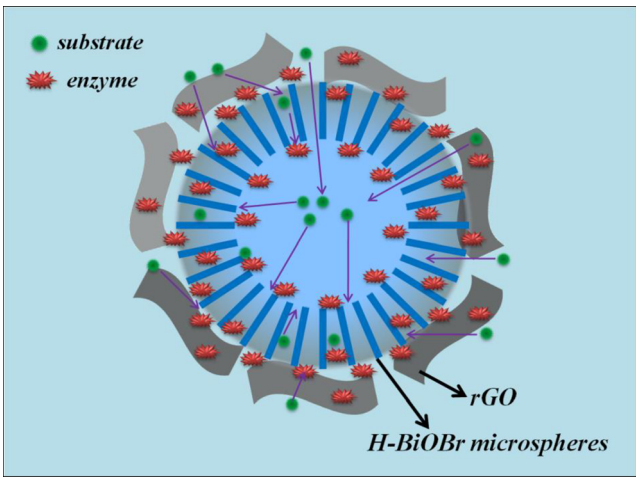

Scheme 1 Schematic illustration of the H-BiOBr/rGO hybrids encapsulating hemoglobin

Experimental

Materials and apparatus

Nafion and Hb solution (5 wt% in lower aliphatic alcohols) are bought from Sigma Co., Ltd., China. Whereas, all other chemicals (analytical grade) are bought from Sinopharm Chemical Reagent Co., Ltd., China. Deionized water is utilized in all experiments. The patterns of X-ray diffraction (XRD) are recorded on a Rigaku D/max 2200 pc diffractometer by Cu Kα radiation of wavelength λ = 0.15418 nm at 40 mA and 40 kV. Field-emission scanning electron microscopy (FE-SEM) is carried out by using a Hiroba energy-dispersive X-ray electron microscope and Hitachi S-4800 (Hitachi, Japan). For transmission electronic microscopy (TEM), FEI Tecnai F20 is employed. UV-vis spectra are documented with a PerkinElmer Lambda-950 spectrophotometer. The CHI 660D electrochemical workstation (CH Instruments, Shanghai, China) is employed to carry out all electrochemical experiments. In all electrochemical experiments, a traditional three-electrode system that comprises a platinum wire as the counter electrode, a 3-mm-diameter modified glassy carbon electrode (GCE) as the functioning electrode and an Ag/AgCl/3M KCl as the reference electrode is utilized. Whereas, in all experiments, 0.1 M phosphate buffered saline (PBS, pH 7.0) is utilized as the supporting electrolyte. For at least 30 min, the buffer is cleansed with extremely purified nitrogen as well as nitrogen atmosphere environment is maintained in electrochemical measurements.

Preparation of reduced graphene oxide

Graphene oxide (GO) was synthesized using graphite powder by means of an altered Hummers method [34]. An ordinary hydrothermal method was used for the preparation of the reduced graphene oxide (rGO). Figure S1 shows the SEM image of GO and rGO along with the Raman spectra of GO (a) and rGO (b).

Synthesis of hollow BiOBr microspheres

In an ordinary experimental procedure, 1.94 g of $Bi(NO_3)_3 \cdot 5H_2O$ was dispersed in a 60 mL mixture of ethanediolglycol and isopropanol with a 2:1 volume ratio. After magnetic stirring for 30 min, 2.91 g of CTAB was added to the mixture under continuous stirring for 1 h. Subsequently, the reaction suspension was transferred into a Teflon-lined autoclave, then hydrothermal treated at 140 °C for 8 h. The resulting precipitate was naturally cooled to room temperature, washed with distilled water and collected after centrifugation. After drying for 10 h at 80 °C in air, the BiOBr precursors were obtained. The ultimate product of white BiOBr was prepared at 400 °C for 4 h in air with a slower heating rate of 5 °C/min.

Preparation of enzyme electrode

Enzyme electrode was collected to examine the electrochemical behavior of Nafion/Hb/H-BiOBr/rGO/GCE. Before utilizing, the GCE were successively polished using 1.0, 0.3 and 0.05 μm alumina powder on a polishing cloth and washed with deionized water. The electrode was therefore sonicated in deionized water along with ethanol. Further, the electrode was dried out by utilizing a purified nitrogen stream. A simple casting method was used for preparing an enzyme electrode. Initially, 0.5 mL of 10 mg mL^{-1} Hb and 1 mL of 2 mg mL^{-1} H-BiOBr MS suspension were blended as well as stirred for 30 min. Further, 0.5 mL of Nafion (5%) and 0.5 mL of rGO (5%) were inserted to the mixture and then stirred for 10 min. Ultimately, 4 μL of the mixture was dropped to the surface of a newly polished GCE to prepare the Nafion/Hb/H-BiOBr/rGO/GCE. The water may evaporate gradually in air as the beaker was sheathed through the electrode, and thus the unified film electrode may be gathered. When the electrode was not utilized, the dried out Nafion/Hb/H-BiOBr/rGO/GCE were stored at 4 °C in a refrigerator.

In comparison, rGO and H-BiOBr MS were utilized for the synthesis of Nafion/Hb/rGO/GCE and Nafion/Hb/H-BiOBr/GCE by the same processes as mentioned above. All the prepared film electrodes were immersed in pH 7.0 PBS for 30 min to eliminate all residuary components prior to electrochemical measurements.

Results and discussion

Characterization of hollow BiOBr-rGO microspheres

The structure of prepared samples was characterized by X-ray diffraction (XRD). Figure 1 shows the typical XRD patterns of the H-BiOBr MS (red curve) and H-BiOBr/rGO hybrids (black curve). The results show that all diffraction peaks of both samples can be assigned to the tetragonal phase of BiOBr (JCPDS card no. 09-0393). The obvious and sharp diffraction peaks of the XRD pattern also indicate that the prepared H-BiOBr MS and H-BiOBr/rGO hybrid samples are well crystalline. Typical SEM and TEM images of the prepared samples were demonstrated in Fig. 2. From Fig. 2a, it is noticed that H-BiOBr MS possess a better control result with dispersion and homogeneity. Figure 2b shows a representative magnified SEM image of H-BiOBr MS. It can be seen clearly that the flower-like hollow microspheres consisted of countless nanometer-sized flakes by self-assembly. Figure 2c puts forward the TEM image of the pure BiOBr MS. It possesses a hollow structure that demonstrates complete coherence with the noticed outcomes of SEM. Flower-like hollow microspheres within a diameter of 2 to 3 μm are tightly self-assembled by the countless chips. The distance between adjacent lattice planes is 0.279 nm, which corresponds to the (110) planes of the tetragonal BiOBr phase. It can be noted from Fig. 2d, e that the morphology of H-BiOBr MS was not altered after the wrapped process. It is shown that dissimilar from that of the pure H-BiOBr MS, the surface of the H-BiOBr/rGO hybrids put forward a wrinkle-like morphology which demonstrates that the surface of H-BiOBr MS was wrapped by rGO nanosheets. Figure 2f depicts the TEM image of the H-BiOBr/rGO hybrids; it can be seen that the H-BiOBr MS was regularly covered by scrunched rGO sheets. The crystallographic spacing of 0.285 nm in the illustration corresponds well with the (102) crystallographic plane of tetragonal

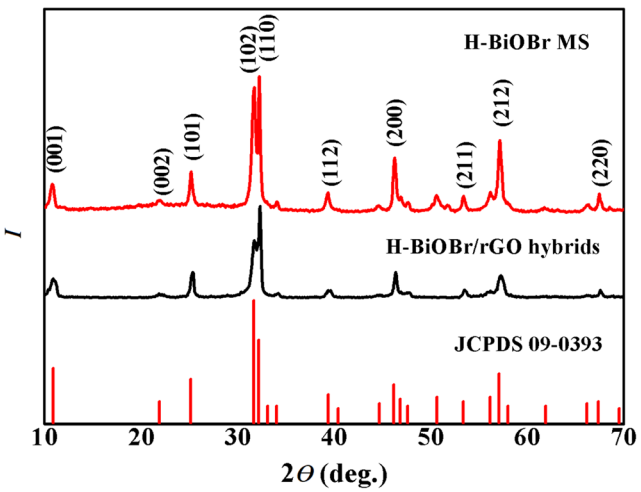

Fig. 1 XRD patterns of H-BiOBr MS (**a**) and H-BiOBr/rGO hybrids (**b**)

BiOBr. The nanometer-scale H-BiOBr MS and rGO possess plenteous active surface area accessible to soak up enzyme and owns well biocompatibility to provide a protective microenvironment for enzyme to maintain its bioactivity. Consequently, the hollow H-BiOBr/rGO hybrids are an extraordinary matrix for enzyme immobilization.

Encapsulation of Hb in the Nafion/Hb/H-BiOBr/rGO composite film

Figure S2 exhibits a typical SEM image of a Nafion/Hb/H-BiOBr/rGO MS composite film. It can be clearly observed that Hb is packaged on H-BiOBr/rGO MS. Due to plenty of laminated space and the hollow structure of the nanomicrosphere, a large amount of Hb can be loaded on the surface and inside of the H-BiOBr/rGO MS. Moreover, the Hb/H-BiOBr/rGO MS were embedded in the Nafion to form a stable composite film, which was essential for the stability of the prepared enzyme electrode.

UV-vis spectroscopy of heme proteins shows a Soret absorption band, and the location of the Soret absorption band can express such information of protein structure like integrity and heme protein denaturation [35, 36]. As demonstrated in Fig. 3a, the Soret absorption band of Hb immobilized in the Nafion/H-BiOBr/rGO film is situated at 404.5 nm (curve a), which is approaching the indigenous Hb at 406 nm (curve c), signifying that Hb maintained the vital characteristics of its conformational integrity. At the same time, the Soret absorption band of Hb immobilized in the Nafion film is situated at 398 nm (curve b in Fig. 3a), which is diverse from that of indigenous Hb, proposing that the Hb is denatured actually. This reveals that the H-BiOBr/rGO hybrids can give a defensive microenvironment for Hb to keep its permanence.

FT-IR spectroscopy is an efficient technique to study the secondary structure of protein macromolecules [37, 38]. The activity of Hb in this study is also analyzed by infrared spectroscopy analysis on the composite film of the electrode surface. In a typical FT-IR spectrum of Hb, the protein has amide I and amide II characteristic absorption bands, which may give

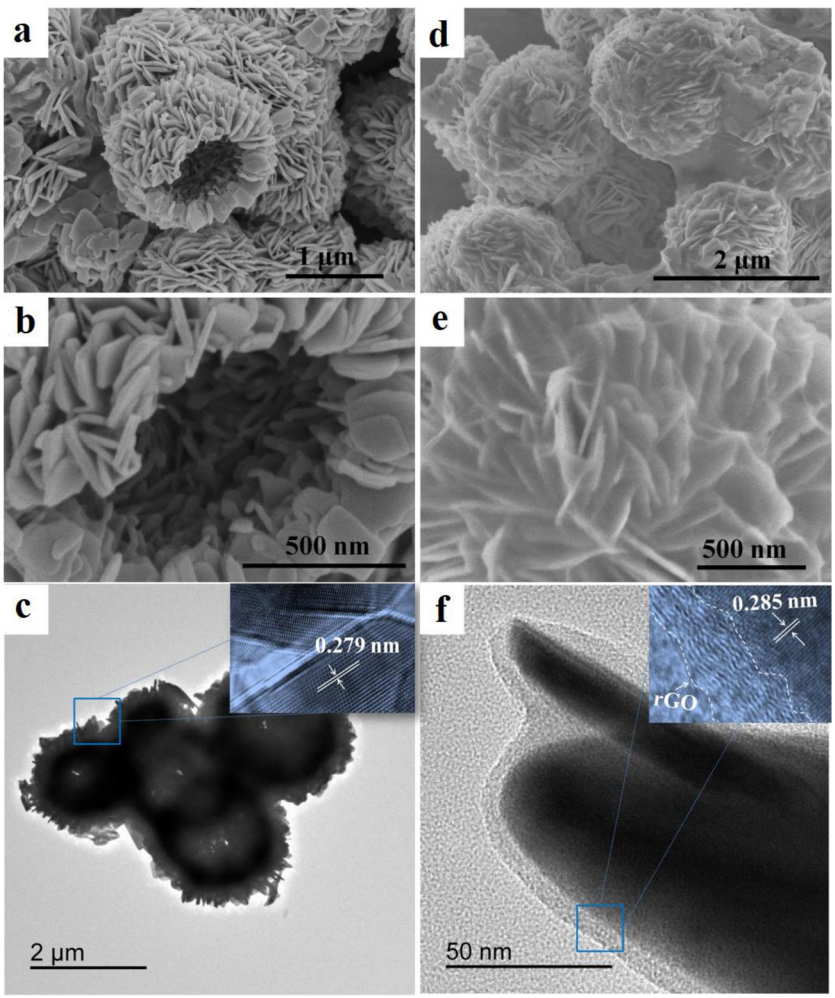

Fig. 2 SEM and TEM images. Low and high-magnification SEM and TEM images of H-BiOBr MS (**a**-**c**) and H-BiOBr/rGO hybrids (**d**-**f**)

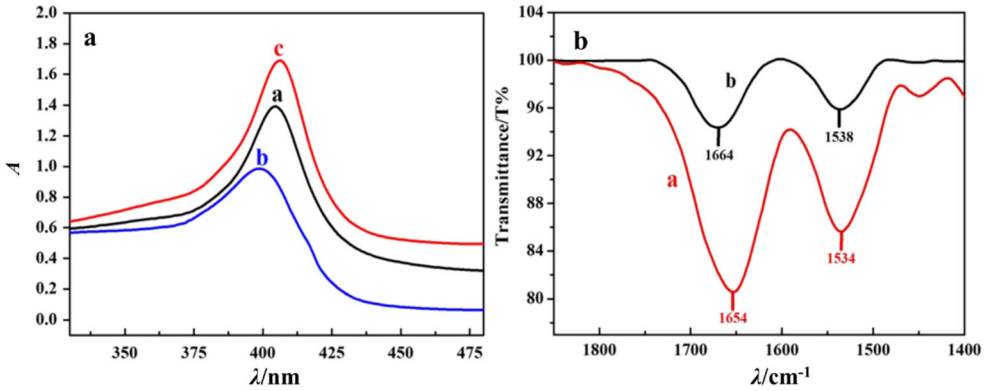

Fig. 3 UV-vis absorption spectra (**a**) of Hb immobilized in Nafion/H-BiOBr/rGO composite film (curve a) and Nafion film (curve b) and native Hb (curve c); FT-IR spectra (**b**) of Hb (curve a) and Nafion/Hb/H-BiOBr/rGO composite film (curve b)

abundant detailed information of polypeptide chain in proteins. In the backbone of protein, the amide I band (1700–1600 cm^{-1}) results from C=O stretching vibration of peptide linkages. The amide II band (1620–1500 cm^{-1}) is due to the amalgamation of N–H bending and C–N stretching. Figure 3b demonstrates the in situ FT-IR spectra of Hb (curve a) and Nafion/Hb/H-BiOBr/rGO composite film (curve b). As we all know, Nafion, which is without peptide linkage, does not contain amide I and amide II absorption peaks. Thus, the spectra of amide I and amide II bands of Hb in the Hb/H-BiOBr/rGO composite film (1664 and 1538 cm^{-1}) are exactly identical with the absorption peak of pure Hb (1654 and 1534 cm^{-1}), suggesting that the native Hb of the composite film essentially keep the secondary structure, consistent results of which were seen in Fig. 3b [39]. The resemblance of two spectra indicates that H-BiOBr/rGO hybrids have an excellent biocompatibility and can give a suitable microenvironment for Hb to keep its biological activity. Such type of H-BiOBr/rGO hybrids with great biocompatibility should be a promising matrix for biosensor fabrication as well as protein immobilization.

Direct electrochemistry behavior of Nafion/Hb/H-BiOBr/rGO/GCE

Figure 4a portrays the usual cyclic voltammograms (CVs) of various modified electrodes in 0.1 M PBS (pH 7.0) at a scan rate of 0.1 V s^{-1}. No redox peak is noted at Nafion/H-BiOBr/rGO/GCE (curve a), which demonstrates Nafion/H-BiOBr/rGO/GCE is electroinactive in the potential window. The Nafion/Hb/H-BiOBr/rGO/GCE (curve e) displays a couple of stable and clearly identified redox peaks at −0.391 V and −0.339 V vs. Ag/AgCl, which can be attributed to direct electron transfer (DET) between Hb and the underlying electrode. As reported by Xu et al. [40], the electron transfer of Hb takes place between the Fe^{III} and Fe^{II} site inset Hb itself. The formalized potential (E^{o} = (E_{pa} + E_{pc}) / 2) of Hb is −0.365 V vs. Ag/AgCl, which is in good arrangement with −0.353 V and −0.348 V reported for the Hb ($Fe^{III/II}$) redox couple in Hb-ZnO-MWCNTs-Nafion [41] and Hb-TiO_2-MXene-Nafion films [42]. The potential difference (ΔE_p) between the cathodic and anodic peak potential is about 52 mV, marginally larger than the theoretical value of the reversible surface appended

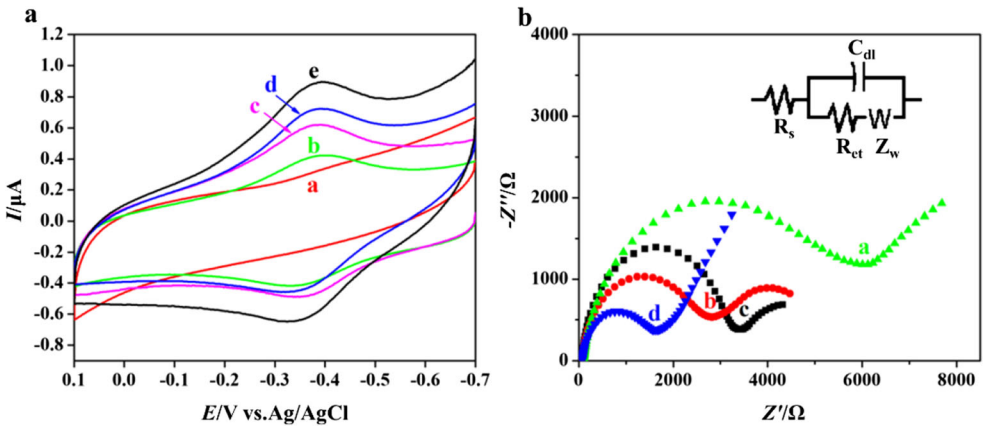

Fig. 4 Cyclic voltammograms (**a**) of Nafion/H-BiOBr/rGO/GCE (curve a), Nafion/Hb/GCE (curve b), Nafion/Hb/rGO/GCE (curve c), Nafion/Hb/H-BiOBr/GCE (curve d) and Nafion/Hb/ H-BiOBr/rGO/GCE (curve e), in 0.1 M pH 7.0 PBS with a scan rate of 0.1 V s^{-1}. EIS (**b**) of Nafion/Hb/GCE (curve a), Nafion/Hb/rGO/GCE (curve b), Nafion/Hb/H-BiOBr/GCE (curve c) and Nafion/Hb/H-BiOBr/rGO/GCE (curve d), in 10 mM $K_3Fe(CN)_6/K_4Fe(CN)_6$ (1:1) containing 0.1 M KCl with the frequencies ranging from 10^5 to 0.1 Hz

reaction process (0 mV) [43], which exposes a quasi-reversible electron-transfer process. It is noticed that the redox peaks of the Nafion/Hb/GCE (curve b in Fig. 4a) are much lower than that of the Nafion/Hb/H-BiOBr/rGO/GCE. As a result of the denaturation of proteins on the bare electrode surface and the acute burying of electroactive center in the protein structure, it is difficult for proteins to realize the DET process on the bare electrode [44]. Clearly, it could be spotted that direct electron transfer between Hb molecules and GCE is significantly improved at the Nafion/Hb/H-BiOBr/rGO/GCE. For comparison, the typical CV test for Nafion/Hb/rGO/GCE and Nafion/Hb/H-BiOBr/GCE has also been performed (curve c and d in Fig. 4a). The intensity of the redox peaks that belong to these electrodes is lower than that of Nafion/Hb/H-BiOBr/rGO/GCE. This may infer that H-BiOBr/rGO hybrids possess a positive promoting effect on electron transfer that might result from their matchless structure as well as electrochemical performance.

Electrochemical impedance spectroscopy (EIS) may provide data on the impedance of different modified electrodes. The semicircular section observed at high frequencies in the Nyquist diagrams matches the electron transfer–limited process, and its diameter is equivalent to an electron transfer resistance. Figure 4b displays the Nyquist plots of the EIS of Nafion/Hb/GCE (curve a), Nafion/Hb/rGO/GCE (curve b), Nafion/Hb/H-BiOBr/GCE (curve c) and Nafion/Hb/H-BiOBr/rGO/GCE (curve d) in 10 mM $K_3Fe(CN)_6$/$K_4Fe(CN)_6$ (1:1) solution including 0.1 M KCl. The electron transfer resistance (R_{et}) of Nafion/Hb/GCE was found to be 5934 Ω. Whereas, the R_{et} values of Nafion/Hb/rGO/GCE and Nafion/Hb/H-BiOBr/GCE were obtained to be 3199 and 3430 Ω, respectively, that were lower than that of Nafion/Hb/GCE. The results indicate that the conductivity of the composite film was improved as a result of the existence of H-BiOBr MS or rGO nanosheets. The R_{et} value of Nafion/Hb/H-BiOBr/rGO/GCE was further reduced to 2255 Ω, signifying that Hb/H-BiOBr/rGO hybrids have the best conductivity.

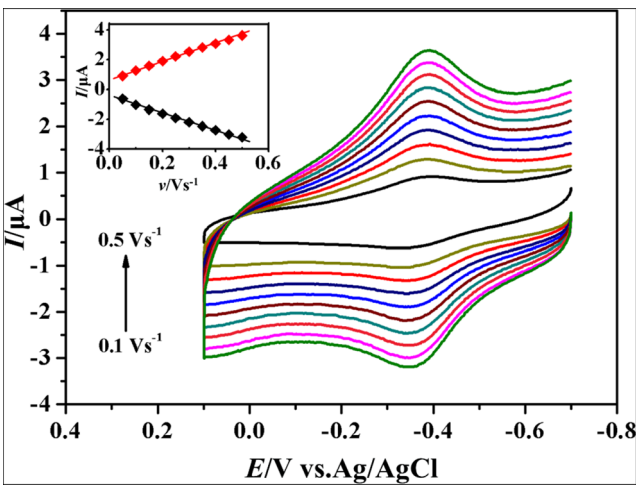

Fig. 5 Cyclic voltammograms of the Nafion/Hb/H-BiOBr/rGO/GCE in 0.1 M pH 7.0 PBS with increasing scan rates from 0.1 to 0.8 V s^{-1}. Inset: plot of the cathodic and anodic peak current vs. scan rate

Figure 5 demonstrates the cyclic voltammograms of Nafion/Hb/H-BiOBr/rGO/GCE at 0.1 M PBS (pH 7.0) with increasing scan rate from 0.1 to 0.5 V s^{-1}. With an enhancement of the scan rate, the anodic as well as cathodic peak currents of Hb enhance concurrently; the anodic and cathodic peak potentials demonstrate a little shift, and the peak-to-peak separation also turns into somewhat augmented. The inset illustration in Fig. 5 demonstrates that both the cathodic (red curve) and anodic (black curve) peak currents show a linear change with scan rates from 0.1 to 0.5 V s^{-1}. This shows that the electrode reaction matches a surface-controlled reaction process. The electron transfer rate constant (k_s) of Hb immobilized in Nafion/Hb/H-BiOBr/rGO/GCE can be evaluated in accordance with Laviron's model if the value of $n\Delta E_P \leq 200$ mV [45]:

$$m = \frac{RT}{F}\frac{k_s}{nv} \tag{1}$$

where m refers to parameter relevant to ΔE_P. The value of k_s is estimated to be around 4.1 s^{-1}, that is larger than the value reported for Hb immobilized Au-SBA-15, 0.8 s^{-1} [46], TiO_2 nanorods-graphene (0.65 s^{-1}) and nitrogen-doped graphene (2.36 s^{-1}) [47], implying a quicker electron transfer process. This further proved that the exceptional structure of H-BiOBr/rGO hybrids is favorable to the quick direct electron transfer of Hb.

Meanwhile, the average surface concentration of electroactive Hb (Γ^*, mol cm^{-2}) can be estimated from the charge integration of the reduction peak of the CV using the formula:

$$Q = nFA\Gamma^* \tag{2}$$

where Q is the charge (C) and may be acquired by integrating the reduction peak of Hb, F is Faraday constant, and A and n refer to the geometrical surface area of the electrode and the number of electron transferred, respectively. In this method, the surface concentration of electroactive Hb (Γ^*) at Nafion/Hb/H-BiOBr/rGO/GCE is computed as 1.16×10^{-10} mol cm^{-2}, much more than the theoretical value for monolayer coverage (1.89×10^{-11} mol cm^{-2}) [48]. This reveals that the multilayers of Hb immobilized in the Nafion/Hb/H-BiOBr/rGO composite film are involved in the electron transfer process. In addition, the Brunner-Emmet-Teller (BET) of H-BiOBr/rGO hybrids and the effective electrochemical active surface area (EASA) of the Nafion/Hb/H-BiOBr/rGO composite film were performed. As shown in Fig. S3, the average specific surface area of H-BiOBr/rGO hybrids is 34.69 m^2/g, which further indicates that the H-BiOBr/rGO hybrids with a higher specific surface area can load more Hb. According to the CV results at different scan rates, the value of EASA for

Nafion/Hb/H-BiOBr/rGO/GCE was estimated to be 1.04 × 10^{-2} cm^{-2}. These results indicated that the unique hollow structure of H-BiOBr/rGO hybrids provides a larger specific surface area for Hb loading.

Figure 6 shows the cyclic voltammograms of Nafion/Hb/H-BiOBr/rGO/GCE at 0.1 M PBS with different pH values. Stable as well as clearly defined CVs have been noticed in the pH range 6.0–8.0. With the increase of the pH value, both the anodic and cathodic peaks transferred to the negative position as shown in Fig. 6a, which is in accordance with the participation of proton transfer in the $Hb(Fe^{III})/Hb(Fe^{II})$ redox couple [49]. Figure 6b exhibited that the $E^{0'}$ value of Hb changes lineally in the range of pH 6.0–8.0, with a slope of −56.5 mV pH^{-1}, which is extremely close to the theoretical value for the transfer of one proton and electron in a reversible reduction (−58 mV pH^{-1} at 25 °C) [50]. Subsequently, it is worth noting that the redox peak current of Hb in PBS with pH = 7.0 is the highest (Fig. 6a), because the higher activity coincides with the inner biological environment.

Electrocatalytic properties of the Nafion/Hb/H-BiOBr/rGO/GCE

Hb displays a typical electrocatalytic reduction reaction for oxygen, H_2O_2, nitrite and Cl_3CCOOH following Hb with maintained bioactivity is immobilized on an electrode surface [38]. In this paper, to study the electrocatalytic property of the Nafion/Hb/H-BiOBr/rGO/GCE, H_2O_2 was chosen as a probe. Figure 7 shows the cyclic voltammograms of Nafion/Hb/H-BiOBr/rGO/GCE at 0.1 M PBS (pH 7.0) with different H_2O_2 concentrations. It can be seen that the reduction peak enhances drastically with the growing of H_2O_2 concentration while the oxidation peak diminishes and finally disappeared with the increasing of the H_2O_2 concentration (form curve a to j). This results demonstrated an obvious electrocatalytic reduction behavior of H_2O_2 on the surface of Nafion/Hb/H-BiOBr/rGO/GCE. A possible reaction mechanism of H_2O_2 catalyzed through the Hb-based electrode is postulated in the following way: [51]

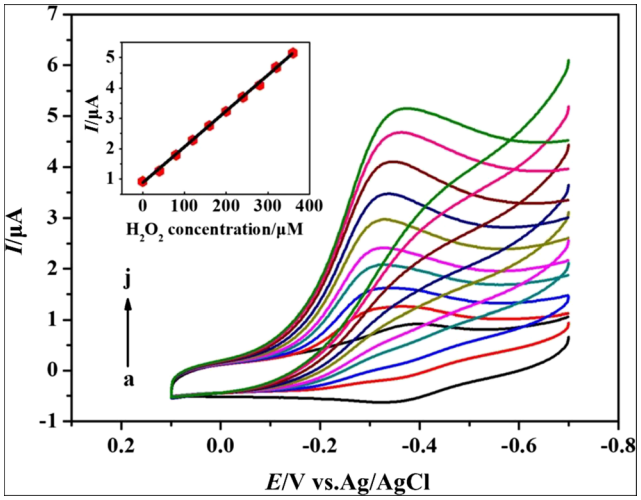

Fig. 7 Cyclic voltammograms of Nafion/Hb/H-BiOBr/rGO/GCE in 0.1 M pH 7.0 PBS containing 0 (**a**), 40 (**b**), 80 (**c**), 120 (**d**), 160 (**e**), 200 (**f**), 240 (**g**), 280 (**h**), 320 (**i**) and 360 (**j**) μM H_2O_2 with a scan rate of 0.1 V s^{-1}. Inset: plot of the cathodic peak current vs. H_2O_2 concentration

$$Hb\left(Fe^{III}\right) + e^{-} \rightleftarrows Hb\left(Fe^{II}\right) \quad (3)$$

$$Hb\left(Fe^{II}\right) + H_2O_2 + 2H^{+} \rightarrow Hb\left(Fe^{III}\right) + 2H_2O \quad (4)$$

With an increasing of H_2O_2 concentration, the present value inclined toward the saturation limit (insertion of Fig. 7). Moreover, the saturating behavior is a characteristic of enzyme-based catalysis. An evident Michaelis-Menten constant (K_M^{app}) could be acquired through an electrochemical version of the Lineweaver-Burk equation: [52]

$$\frac{1}{I_{ss}} = \frac{K_M^{app}}{I_{max}C} + \frac{1}{I_{max}} \quad (5)$$

where C is the bulk concentration of the substrate, I_{max} is the maximum current value assessed underneath saturated substrate conditions and I_{ss} is the stable-state current value following an addition of substrate. The K_M^{app} value can effectively reflect the affinity between the enzyme and the substrate,

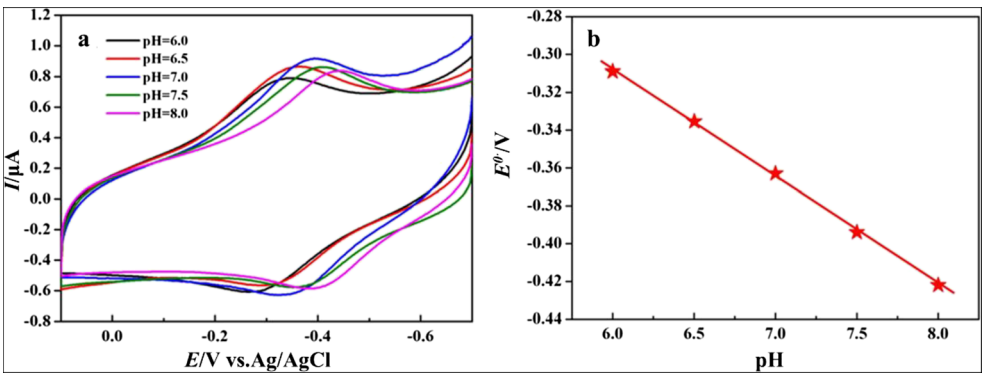

Fig. 6 **a** Cyclic voltammograms of the Nafion/Hb/H-BiOBr/rGO/GCE in 0.1 M PBS with different pH values from 6.0, 6.5, 7.0, 7.5, to 8.0. **b** Plot of formal potential vs. pH value

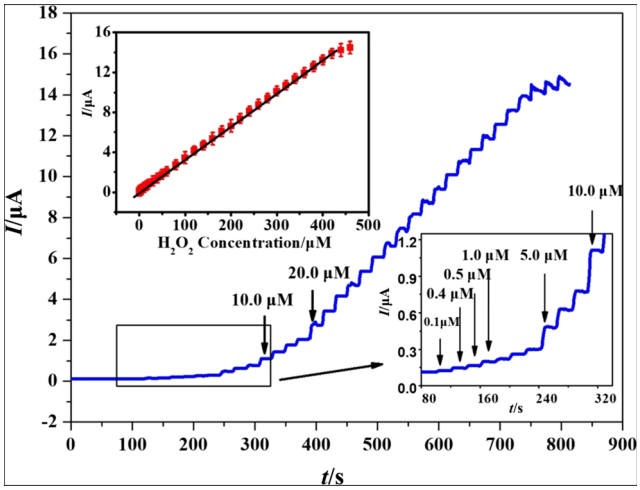

Fig. 8 Typical current-time response of Nafion/Hb/H-BiOBr/rGO/GCE at −0.35 V to successive addition of H_2O_2 in stirred 0.1 M pH 7.0 PBS. Inset: The steady-state current vs. H_2O_2 concentration

and the smaller the K_M^{app} value, the greater the affinity. The K_M^{app} value of Nafion/Hb/H-BiOBr/rGO/GCE is evaluated to be 129.7 μM. This value is lower in comparison to those ever stated values of 379 μM [53] and 684 μM [54], indicating that Nafion/Hb/H-BiOBr/rGO/GCE maintained greater bioactivity as well as grasped the higher biological affinity to H_2O_2.

Biosensor performance of the Nafion/Hb/H-BiOBr/rGO/GCE

The biosensor efficiency for detecting the H_2O_2 of the Nafion/Hb/H-BiOBr/rGO/GCE was also examined over the amperometry method. As a result of its powerful impact on the biosensor feedback, the optimal applied potential has been affirmed earlier through an experiment. Figure 8 gives the typical current-time response of Nafion/Hb/H-BiOBr/rGO/GCE at −0.35 V after the addition of H_2O_2 in the stirred PBS solution (0.1 M, pH 7.0). The response time is less than 3 s when the reduction current rapidly increases to 96% of steady-state current. A clearly defined linear correlation between the current and the H_2O_2 concentration is noticed. The experimental result demonstrated that the Nafion/Hb/H-BiOBr/rGO/GCE has an evident catalyzed effect on H_2O_2. The calibration plot (inset of Fig. 8) demonstrates a linear range of 0.1 to 420 μM (correlation coefficient of 0.998, N = 32) with a susceptibility of 395.8 μA mM^{-1} cm^{-2} and a detection limit of 0.02 μM (on the basis of a signal-to-noise ratio of 3). Moreover, Table S1 shows the comparison of the performances of the various electrochemical biosensors for H_2O_2. It can be seen that the Nafion/Hb/H-BiOBr/rGO/GCE has not just lower detection limit but keeps a comparatively broader linear range, which can be attributed to an extraordinary biocompatibility as well as good electrical conduction of the H-BiOBr/rGO hybrids. Meanwhile, compared with other prepared modified electrodes in this study, both Nafion/Hb/rGO/GCE (curve b) and Nafion/Hb/H-BiOBr/GCE (curve c), Nafion/Hb/H-BiOBr/rGO/GCE (curve a) has the better electrocatalytic performances (Fig. S4 and Table S2).

There exist few reasons why the Nafion/Hb/H-BiOBr/rGO/GCE shows both lower detection limit and broader linear range. Firstly, plenty of enzymes are enabled to be immobilized due to the hollow microsphere structure. Secondly, the laminar microstructure of H-BiOBr MS may significantly improve the active surface area accessible for immobilizing Hb and also keep enzymatic activity as well as stability of Hb. Most significantly, the substrate could merely be entangled by rGO with a higher surface area, allowing the accessibility of a huge amount of enzymes immobilized in the H-BiOBr MS. The concentration of enzyme and substrate in that limited microenvironment would enhance the opportunity of effectual collisions among them. Furthermore, rGO with finer mobility of charge carriers may also become the remarkable media of effectual electrical communication between the electrode and the enzyme.

Selectivity of the H_2O_2 biosensor

For practical utilization of the as-prepared biosensors, selectivity is significant. The selectivity of the biosensor is assessed by utilizing the amperometric current-time method among nine ordinary interfering substances: (a) ascorbic acid, (b) dopamine, (c) uric acid, (d) glucose, (e) glycine, (f) citric acid, (g) acetic acid, (h) $MgSO_4$ solutions and (i) NaCl solutions. When viewed in (Fig. S5), nine tested substances never interfere with the result of H_2O_2 testing substantially. This result may be ascribed to the inherent selectivity of Hb for its substances.

Table 1 Determination of the results of H_2O_2 in real samples

Samples	$KMnO_4$ titration (mM)	This work (mM)	Added (mM)[a]	Found (mM)[b]	Recovery (%)
1	0.15	0.15	0.10	0.22	92.7
2	0.20	0.18	0.10	0.24	96.8
3	0.25	0.24	0.10	0.26	103.8

[a] Standard H_2O_2 solution added to the samples

[b] The total concentrations of H_2O_2 after addition of standard H_2O_2 solution to the samples

Stability and reproducibility of the biosensor

Cycle stability is an essential assessment index for estimating the efficiency of the biosensor; 100 times uninterrupted cyclic scans on Nafion/Hb/H-BiOBr/rGO/GCE have been replicated in the potential range from −0.7 to 0.1 V at a scan rate of 0.1 V s^{-1} (Fig. S6). No apparent change of CV curves is noticed. Thus, the prepared Nafion/Hb/H-BiOBr/rGO/GCE owns an extraordinary cycle stability. The modified electrode was studied by exploring its current feedback later at 4 °C in the refrigerator, and it retained 95.7% of the preliminary feedback to H_2O_2 after 4-week storage. The experimental result shows that the immobilized Hb in Nafion/Hb/H-BiOBr/rGO/GCE could maintain its biological activity for a long time. The reason why fabricated biosensors possessed a nice long-term stability is that the long-term stability might be assigned to the great biocompatibility of H-BiOBr MS, which may offer a favorable microenvironment for Hb to keep its bioactivity. The reproducibility of the biosensor was investigated by determining 10 μM H_2O_2 in PBS (pH 7.0). For 5 consecutive measurements, the relative standard deviation (RSD) is 2.9%. Parallel to the tests of the 5 groups of the same Nafion/Hb/H-BiOBr/rGO/GCE, obtaining a RSD of 3.7% for the determination of 100 μM H_2O_2 in PBS (pH 7.0) signifies an admissible reproducibility.

Analysis of real samples

To investigate the practical applications of the biosensors, the detection of H_2O_2 in contact lens care solution samples was carried out. Prior to experiments, the actual specimens are diluted 4000 times with dually distilled water and excluding any other processes. The $KMnO_4$ titration method and restoration tests were utilized to investigate the dependability and precision of this method. The H_2O_2 content for diverse specimens and restorations of inserted analyte are assessed, and the results affirm that determination of the H_2O_2 concentration in actual specimens by utilizing the suggested method is trustworthy (Table 1).

Conclusion

Hollow BiOBr microspheres have been synthesized through an easy synthetic route with a well-defined morphology immobilizing Hb. To construct a mediator-free biosensor for the detection of H_2O_2, it has been utilized to modify glassy carbon electrode with reduced graphene oxide. More Hb can be immobilized by the special hollow structure of microspheres with biological activity, and the graphene can merely capture the substrate. Consequently, there is an increased opportunity of efficient collisions between redox protein and substrate results in enhanced efficiency of this sensor. On one hand, for H-BiOBr/rGO hybrids with a favorable biocompatibility, it is accessible for immobilizing Hb and keeps enzymatic stability as well as activity of Hb. On the other hand, the substrate could merely be entangled by rGO with a higher surface area, allowing the accessibility of a huge quantity of enzymes immobilized in the H-BiOBr/rGO hybrids. As a result of the aforementioned reasons, the constructed mediator-free biosensors show an exceedingly low limit of detection of 0.02 μM and a broad linear range of 0.1–420 μM. This study shows that H-BiOBr/rGO hybrid is a potential matrix for enzyme immobilization and the construction of a direct electrochemical biosensor.

Supplementary Information The online version contains supplementary material available at https://doi.org/10.1007/s10008-021-04958-2.

Funding We acknowledge financial support from the Foundation for Young Scholars of Shaanxi University of Science & Technology (No. 2017BJ-06), the Natural Science Foundation of Shaanxi Province (No. 2018JQ2069), the Scientific Research Program funded by the Shaanxi Provincial Education Department (No. 18JK0113) and the Graduate Innovation Fund of Shaanxi University of Science & Technology.

References

1. Hosseini H, Behbahani M, Mahyari M, Kazerooni H, Bagheri A, Shaabani A (2014) Ordered carbohydrate-derived porous carbons immobilized gold nanoparticles as a new electrode material for electrocatalytical oxidation and determination of nicotinamide adenine dinucleotide. Biosens Bioelectron 59:412–417
2. Bojdi MK, Mashhadizadeh MH, Behbahani M, Farahani A, Davarani SSH, Bagheri A (2014) Synthesis, characterization and application of novel lead imprinted polymer nanoparticles as a high selective electrochemical sensor for ultra-trace determination of lead ions in complex matrixes. Electrochim Acta 136:59–65
3. Kalate BM, Behbahani M, Mashhadizadeh MH, Bagheri A, Hosseiny Davarani SS, Farahani A (2015) Mercapto-ordered carbohydrate-derived porous carbon electrode as a novel electrochemical sensor for simple and sensitive ultra-trace detection of omeprazole in biological samples. Mater Sci Eng C 48:213–219
4. Xu F, Wang PF, Lin M, Lu TJ, Ng EYK (2010) Quantification and the underlying mechanism of skin thermal damage. J Mech Med Biol 10(03):373–400
5. Baghayeri M, Nazarzadeh ZE, Hasanzadeh R (2014) Facile synthesis of PSMA-g-3ABA/MWCNTs nanocomposite as a substrate for hemoglobin immobilization. Mater Sci Eng C Mater Biol Appl 39:213–220
6. Baghayeri M, Veisi H, Farhadi S, Beitollahi H, Maleki B (2018) Ag nanoparticles decorated Fe_3O_4/chitosan nanocomposite. J Iran Chem Soc 15(5):1015–1022
7. Baghayeri M, Zare EN, Lakouraj MM (2014) Novel superparamagnetic PFu@Fe_3O_4 conductive nanocomposite as a suitable host for hemoglobin immobilization. Sensors Actuators B Chem 202:1200–1208
8. Léger C, Elliott SJ, Hoke KR, Jeuken LJ, Jones AK, Armstrong FA (2003) Enzyme electrokinetics: using protein film voltammetry to investigate redox enzymes and their mechanisms. Biochemistry 42(29):8653–8662

9. Hamachi I, Akio Fujita A, Kunitake T (1997) Protein engineering using molecular assembly: functional conversion of cytochrome c via noncovalent interactions. J Am Chem Soc 11:83–84
10. Zhu Z, Qu L, Niu Q, Zeng Y, Sun W, Huang X (2011) Urchinlike MnO nanoparticles for the direct electrochemistry of hemoglobin with carbon ionic liquid electrode. Biosens Bioelectron 26(5): 2119–2124
11. Sheng QL, Zheng JB, Shang-Guan XD, Lin WH, Li YY, Liu RX (2010) Direct electrochemistry and electrocatalysis of heme-proteins immobilized in porous carbon nanofiber/room-temperature ionic liquid composite film. Electrochim Acta 55(9): 3185–3191
12. Kim J, Grate JW, Wang P (2006) Nanostructures for enzyme stabilization. Chem Eng Sci 61(3):1017–1026
13. Zhang L, Zhang Q, Li J (2007) Direct electrochemistry and electrocatalysis of hemoglobin immobilized in bimodal mesoporous silica and chitosan inorganic–organic hybrid film. Electrochem Commun 9(7):1530–1535
14. Huang X, Li Y, Zhou H, Zhong X, Duan X, Huang Y (2012) Simplifying the creation of dumbbell-like Cu-Ag nanostructures and their enhanced catalytic activity. Chemistry 18(31):9505–9510
15. Mahmoud MA, El-Sayed MA (2012) Metallic double shell hollow nanocages: the challenges of their synthetic techniques. Langmuir Acs J Surf Colloids 28(9):4051–4059
16. Yang Y, Matsubara S, Nogami M, Shi J, Huang W (2006) One-dimensional self-assembly of gold nanoparticles for tunable surface plasmon resonance properties. Nanotechnology 17(11):2821–2827
17. Cao Y, Zou X, Wang X, Qian J, Bai N, Li GD (2016) Effective detection of trace amount of explosive nitro-compounds by ZnO nanofibers with hollow structure. Sensors Actuators B Chem 232: 564–570
18. Li XZ, Wu KL, Dong C, Xia SH, Ye Y, Wei XW (2014) Size-controlled synthesis of Ag_3PO_4 nanorods and their high-performance photocatalysis for dye degradation under visible-light irradiation. Mater Lett 130:97–100
19. Cheng H, Huang B, Dai Y (2014) Engineering BiOX (X = Cl, Br, I) nanostructures for highly efficient photocatalytic applications. Nanoscale 6(4):2009–2026
20. And GGB, Burford N (1999) Bismuth compounds and preparations with biological or medicinal relevance. Chem Rev 99:2601–2658
21. Li J, Yu Y, Zhang L (2014) Bismuth oxyhalide nanomaterials: layered structures meet photocatalysis. Nanoscale 6(15):8473–8488
22. Liang W, Jia TF, Xin Y, Li CH, Feng LJ (2016) Hydrothermal synthesis of BiOBr/semi-coke composite as an emerging photocatalyst for nitrogen monoxide oxidation under visible light. Catal Today 264:257–260
23. Yin Y, Qian L, Ding J, Du X, Jing Q, Mao H, Wang K (2016) Atmospheric pressure synthesis of nitrogen doped graphene quantum dots for fabrication of BiOBr nanohybrids with enhanced visible-light photoactivity and photostability. Carbon 96:1157–1165
24. Li L, Ai L, Zhang C, Jiang J (2014) Hierarchical {001}-faceted BiOBr microspheres as a novel biomimetic catalyst: dark catalysis towards colorimetric biosensing and pollutant degradation. Nanoscale 6(9):4627–4634
25. Chen J, Guan M, Cai W, Guo J, Xiao C, Zhang G (2014) The dominant {001} facet-dependent enhanced visible-light photoactivity of ultrathin BiOBr nanosheets. Phys Chem Chem Phys Pccp 16(38):20909–20914
26. Zhou Q, Yang L, Wang G, Yang Y (2013) Acetylcholinesterase biosensor based on SnO_2 nanoparticles-carboxylic graphene-nafion modified electrode for detection of pesticides. Anal Biochem 49: 25–31
27. Yang L, Wang G, Liu Y, Wang M (2013) Development of a biosensor based on immobilization of acetylcholinesterase on NiO nanoparticles-carboxylic graphene-nafion modified electrode for detection of pesticides. Talanta 113:135–141
28. Chen YX, Huang KJ, He LL, Wang YH (2018) Tetrahedral DNA probe coupling with hybridization chain reaction for competitive thrombin aptasensor. Biosens Bioelectron 100:274–281
29. Liu J, Wang Y, Hu R, Munir HA, Liu H (2020) High-performance supercapacitor electrode based on 3D rose-like β-$Ni(OH)_2$/rGO nanohybrid. J Phys Chem Solids 138:109297
30. Shuai HL, Wu X, Huang KJ (2017) Molybdenum disulfide spheres-based electrochemical aptasensor for proteins detection. J Mater Chem B 5(27):5362–5372
31. Wang YH, Chen YX, Wu X, Huang KJ (2018) Electrochemical biosensor based on Se-doped MWCNTs-graphene and Y-shaped DNA-aided target-triggered amplification strategy. Colloids Surf B: Biointerfaces 172:407–413
32. Wang YH, Huang KJ, Wu X, Ma YY, Song DL, Du CY, Chang SH (2018) Ultrasensitive supersandwich-type biosensor for enzyme-free amplified microRNA detection based on N-doped graphene/Au nanoparticles and hemin/G-quadruplexes. J Mater Chem B 6(14):2134–2142
33. Xie Q, Zhao Y, Chen X, Liu H, Evans DG, Yang W (2011) Nanosheet-based titania microspheres with hollow core-shell structure encapsulating horseradish peroxidase for a mediator-free biosensor. Biomaterials 32(27):6588–6594
34. Kovtyukhova NI, Ollivier PJ, Martin BR, Mallouk TE, Gorchinskiy AD (1999) Layer-by-layer assembly of ultrathin composite films from micron-sized graphite oxide sheets and polycations. Chem Mater 11(3):771–778
35. Mao S, Long Y, Li W, Tu Y, Deng A (2013) Core-shell structured Ag@C for direct electrochemistry and hydrogen peroxide biosensor applications. Biosens Bioelectron 48:258–262
36. Chen X, Fu C, Wang Y, Yang W, Evans DG (2008) Direct electrochemistry and electrocatalysis based on a film of horseradish peroxidase intercalated into Ni-Al layered double hydroxide nanosheets. Biosens Bioelectron 24(3):356–361
37. Sun W, Guo Y, Ju X, Zhang Y, Wang X, Sun Z (2013) Direct electrochemistry of hemoglobin on graphene and titanium dioxide nanorods composite modified electrode and its electrocatalysis. Biosens Bioelectron 42:207–213
38. Lu X, Zhang H, Ni Y, Zhang Q, Chen J (2008) Porous nanosheet-based ZnO microspheres for the construction of direct electrochemical biosensors. Biosens Bioelectron 24(1):93–98
39. Yu J, Ma T, Liu S (2011) Enhanced photocatalytic activity of mesoporous TiO_2 aggregates by embedding carbon nanotubes as electron-transfer channel. Phys Chem Chem Phys 13(8):3491–3501
40. Xu Q, Mao C, Liu NN, Zhu JJ, Sheng J (2006) Direct electrochemistry of horseradish peroxidase based on biocompatible carboxymethyl chitosan-gold nanoparticle nanocomposite. Biosens Bioelectron 22(5):768–773
41. Ma W, Tian D (2010) Direct electron transfer and electrocatalysis of hemoglobin in ZnO coated multiwalled carbon nanotubes and Nafion composite matrix. Bioelectrochemistry 78(2):106–112
42. Wang F, Wang Z, Zhu J, Yang H, Chen X, Wang L, Yang C (2017) Facile synthesis SnO_2 nanoparticle-modified Ti_3C_2 MXene nanocomposites for enhanced lithium storage application. J Mater Sci 52:1–10
43. Hui L, Duan C, Yang C, Shen W, Wang F, Zhu Z (2015) A novel nitrite biosensor based on the direct electrochemistry of hemoglobin immobilized on MXene-Ti_3C_2. Sensors Actuators B Chem 218:60–66
44. Liu H, Duan C, Yang C, Chen X, Shen W, Zhu Z (2015) A novel nitrite biosensor based on the direct electron transfer hemoglobin immobilized in the WO_3 nanowires with high length–diameter ratio. Mater Sci Eng C Mater Biol Appl 53:43–49

45. Yang X, Chen X, Yang L, Yang W (2008) Direct electrochemistry and electrocatalysis of horseradish peroxidase in alpha-zirconium phosphate nanosheet film. Bioelectrochemistry 74(1):90–95
46. Xian Y, Xian Y, Zhou L, Wu F, Ling Y, Jin L (2007) Encapsulation hemoglobin in ordered mesoporous silicas: influence factors for immobilization and bioelectrochemistry. Electrochem Commun 9(1):142–148
47. Sun W, Dong L, Deng Y, Yu J, Wang W, Zhu Q (2014) Application of N-doped graphene modified carbon ionic liquid electrode for direct electrochemistry of hemoglobin. Mater Sci Eng C Mater Biol Appl 39:86–91
48. Wang SF, Chen T, Zhang ZL, Shen XC, Lu ZX, Pang DW, Wong KY (2005) Direct electrochemistry and electrocatalysis of heme proteins entrapped in agarose hydrogel films in room-temperature ionic liquids. Langmuir 21(20):9260–9266
49. Chen X, Wang Q, Wang L, Gao F, Wang W, Hu Z (2015) Imidazoline derivative templated synthesis of broccoli-like Bi_2S_3 and its electrocatalysis towards the direct electrochemistry of hemoglobin. Biosens Bioelectron 66:216–223
50. Wu F, Xu J, Tian Y, Hu Z, Wang L, Xian Y, Jin L (2008) Direct electrochemistry of horseradish peroxidase on TiO_2 nanotube arrays via seeded-growth synthesis. Biosens Bioelectron 24(2): 198–203
51. George S, Lee HK (2009) Direct electrochemistry and electrocatalysis of hemoglobin in Nafion/carbon nanochip film on glassy carbon electrode. J Phys Chem B 113(47):15445–15454
52. Kamin RA, Wilson GS (1980) Rotating ring-disk enzyme electrode for biocatalysis kinetic studies and characterization of the immobilized enzyme layer. Anal Chem 52(8):1198–1205
53. Sun A, Zheng J, Sheng Q (2011) A novel hydrogen peroxide biosensor based on the PDDA-GNPs/MWNTs nanocomposite matrix. J Chin Chem Soc 58(7):857–862
54. Zhang L, Cheng H, Zhang HM, Qu L (2012) Direct electrochemistry and electrocatalysis of horseradish peroxidase immobilized in graphene oxide-Nafion nanocomposite film. Electrochim Acta 65: 122–126